Tumor Growth Estimation via Registration of DCE-MRI Derived Tumor Specific Descriptors

Thaís Roque[1], Bartłomiej W. Papież [1], Veerle Kersemans[2],
Sean Smart[2], Danny Allen[2], Michael Chappell[1], Julia A. Schnabel[1,3]
[1]Institute of Biomedical Engineering, Department of Engineering Science,
University of Oxford, UK
[2]Preclinical Imaging Group, Department of Oncology,
University of Oxford, UK
[3]Department of Biomedical Engineering, Division of Imaging Sciences and Biomedical Engineering,
King's College London, UK
thais.roque@eng.ox.ac.uk

Abstract

Dynamic contrast-enhanced magnetic resonance imaging (DCE-MRI) provides information on changes occurring during tumor growth in the tumor micro-environment and vasculature. In the present paper, tumor voxel-wise estimates of tumor descriptors including total cell number, proliferative cell number, hypoxic cell number, necrotic cell number and oxygen level derived from DCE-MRI data are used to guide the deformable registration of subsequent time points over the tumor growth cycle, evaluating their predictive value for tumor growth. The analysis of three preclinical colon carcinoma longitudinal cases shows that using physiologically meaningful measures of tumor as guidance information can improve non-rigid registration of longitudinal tumor imaging data when compared to a state-of-the-art local correlation coefficient Demons approach. Moreover, using the determinant of the Jacobian of the estimated displacement field as an indicator of volume change allows us to observe a correlation between the tumor descriptor values and tumor growth, especially when maps of hypoxic cells and level of oxygen were used to aid registration. To the best of our knowledge, this work demonstrates for the first time the feasibility of using biologically meaningful tumor descriptors (total cell number, proliferative cell number, hypoxic cell number, necrotic cell number and oxygen level) derived from DCE-MRI to aid non-rigid registration of longitudinal tumor data as well as to estimate tumor growth.

1. Introduction

Although a variety of deformable registration approaches exist in the literature [14], their application in the presence of tissue-modifying pathologies such as tumors remains challenging. The poor registration outcome in the presence of tumors is mainly due to changes caused by tissue death and tumor growth, which do not agree with the assumption of smoothness of the deformation fields [21]. Here, we explore whether the integration of tumoral local physiological information derived from quantitative medical imaging can improve the registration accuracy while allowing for more accurate quantification of local and total tumor growth than the one offered by the state-of-the-art Response Evaluation Criteria in Solid Tumors (RECIST) [18], which determines tumor progression and regression based on the evolution of the longest diameter. The simplicity of this evaluation technique contrasts sharply with the heterogeneity of tumor tissue. Here, the increasing sophistication of medical imaging instrumentation can serve as a major opportunity to add volumetric anatomical and functional information to the tumor burden assessment.

Magnetic Resonance Imaging (MRI) can be used to non-invasively assess tumor tissue heterogeneity. Depending on the technique used, MRI is sensitive to small-vessel structures, which allows for extraction of information on perfusion, tissue oxygenation and metabolism. One of these techniques, dynamic contrast-enhanced magnetic resonance imaging (DCE-MRI), which consists of acquiring several sequential T1-weighted MR images over a short period of time upon the injection of a contrast agent (CA), is able to characterize tumor tissue and its response to therapy as a complement to image acquisition.

The dynamics of the CA can be evaluated based on different models. The first generation of DCE-MRI models, referred to as Tofts models, dates back to the works of Tofts and colleagues in the 1990s [16, 17]. With this model, parameters related to perfusion (i.e. blood delivery to a capillary bed) are obtained by fitting of the CA concentration curves to a pharmacokinetic tracer analysis model. Model-free approaches, in contrast, derive empirical parameters that characterize the shape and structure of the signal intensity time to quantify tissue perfusion.

In the context of analysis of DCE-MRI tumor data, deformable image registration has been mostly used as a tool for motion correction to enable quantitative analysis. Hamy et al. extended a generic registration framework by using a statistical prior derived from a robust DCE-MRI decomposition to constrain the similarity measure during estimation of the displacement field [6]. In [9], Hodneland et al. proposed a joint segmentation and registration driven approach to estimate glomerular filtration rate from DCE-MRI of kidney. A registration algorithm able to simultaneously perform motion correction and pharmacokinetic estimation in DCE-MRI data was proposed by Bhushan et al. in [3]. Their approach incorporated a physiological image formation model directly into the similarity measure, improving the alignment of the images. None of these approaches has been used for preclinical studies.

In this paper, we analyse DCE-MRI data coming from preclinical studies where the presence of tumor is significant. In such cases, neither a generic regularisation model, such as Gaussian regularisation used in [3], nor linear elastic regularisation [9] reflects well the heterogeneity of tumor growth. To address this limitation, to aid the longitudinal 3D registration of tumors, we propose to use DCE-MRI perfusion related parameters (hereafter called *descriptors*), which describe the tumor as a living matter, to form a biologically inspired regularisation model with enhanced registration accuracy and estimation of tumor volume.

The basic components of the proposed methods including the acquisition of the DCE-MRI pre-clinical data, the extraction of the DCE-MRI related tumor descriptors, the deformable image registration method and the use of the tumor descriptors to aid registration are outlined in Section 2. The results are presented in Section 3, and include the registration output and the assessment of tumor volume evolution based on the determinant of the Jacobian of the estimated displacement field for three longitudinal pre-clinical tumor cases. An analysis of the results, an outline of the main contributions and limitations of the proposed method as well as an outlook for future steps are given in Section 4.

2. Methods

2.1. DCE-MRI Based Descriptor Maps Estimation

A combination of model-free deconvolution and semi-quantitative approaches was used to compute DCE-MRI related quantities. The perfusion F was computed by deconvolving the measured gadolinium concentration time curve ($C_t(t)$) with the arterial input function (AIF) using a block-circulant singular value decomposition (oSVD) as described in [19]. The distribution volume v_D, which represents the fraction of tissue accessible to the CA, was computed using a population based AIF [8, 12] and Eq. 1 [15]:

$$v_D = \frac{\int_0^\infty C_t(t)dt}{\int_0^\infty C_a(t)dt} \tag{1}$$

Using the central-volume theorem [22], the mean transit time MTT, which relates v_D to the arterial inlet to the space carrying the plasma flow through each voxel, can be computed as $MTT = v_D/F$.

These parameters offer insight into the tumor metabolic status as well as into its microenvironment and are further converted to physiological parameters (*e.g.* cell density, mitotic activity and oxygenation level), which can be meaningfully used to inform a non-rigid registration approach.

The first tumor descriptor included in this study is an estimate of the number of cells. Contrary to [2], where this descriptor is estimated with the help of two imaging modalities (DW-MRI, which provides a non-invasive measurement of the degree of random motion of water molecules in tissue, and DCE-MRI), we propose a method based on parameters derived solely from DCE-MRI.

In order to estimate the number of tumor cells ($cell$), we assume that the higher the number of cells the longer it will take for the CA to leave the voxel. Hence, a positive correlation between $cell$ and MTT is assumed, which yields $cell = (MTT/MTT_{max}) \cdot (1 - v_D) \cdot capacity$. Where MTT_{max} represents the maximum MTT value found over the whole image, so that MTT/MTT_{max} results in a relative MTT value between 0 and 1. The $capacity$ equals the voxel volume divided by the volume of each tumor cell, which is assumed to be a sphere with a diameter of $10\mu m$.

Tumor cells can be either proliferating (mitosis), quiescent (hypoxia) or necrotic. The number of tumoral cells constituting each group is estimated according to the metabolic activity within the voxel.

The number of proliferating cells is assumed to be proportional to the maximum enhancement peak (mEP) of the concentration time curve ($CTC(t)$) based on findings by [5], where a positive correlation between the mitotic index and mEP could be demonstrated. For each voxel the fraction of proliferating cells can be estimated assuming the relationship $cell_p = cell \cdot \frac{mEP}{mEP_{max}}$.

Cells within a voxel that are not proliferating can either

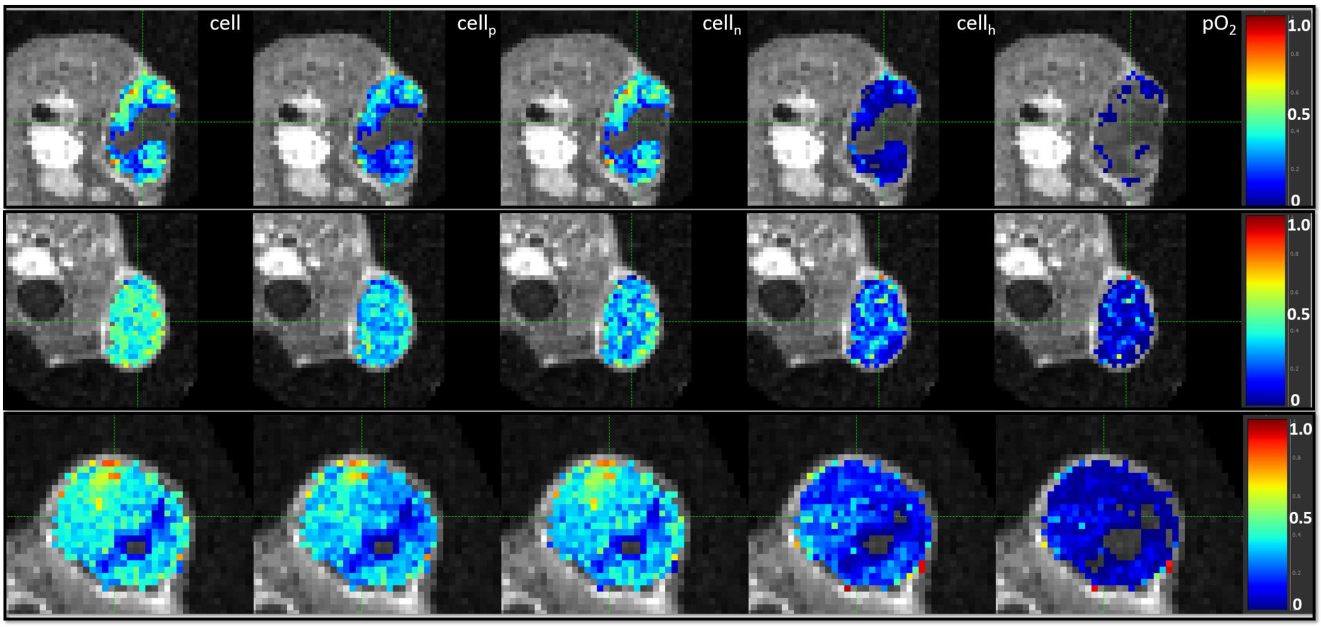

Figure 1. Axial view of tumor descriptor maps relative cell ($cell$), proliferative ($cell_p$), necrotic ($cell_n$) and hypoxic ($cell_h$), and relative oxygen level (pO_2) for τ_2 for Case 1 (top row), Case 2 (middle row) and Case 3.

be hypoxic or necrotic. To obtain the initial fraction of the necrotic cells in each voxel, we assume that low perfusion, and hence low nutrient availability, results in high cell death rate. Making use of this assumption and $cell_p$ yields $cell_n = (cell - cell_p) \cdot \left(1 - \frac{F}{F_{max}}\right)$. The fraction of hypoxic cells in each voxel can be thus estimated using $cell_h = cell - cell_p - cell_n$.

Due to the importance of oxygen delivery to cell survival, it is necessary to extract a tissue oxygen tension (pO_2) map able to provide insight into the tumor's local metabolism. To extract a pO_2 map for each case based on DCE-MRI images, we apply the relationship derived in [1] between pO_2 and the microvessel density (MVD) and assume that v_D is directly related to MVD, so that:

$$pO_2(v_D) = \frac{60 \cdot (K_{pO_2} \cdot v_D)^{1.95}}{(K_{pO_2} \cdot v_D)^{1.95} + 0.015^{1.95}} \qquad (2)$$

where K_{pO_2} is the proportionality constant and has been calibrated to deliver the maximum pO_2 value (60mmHg) at the maximum v_D value over the whole image.

2.2. Deformable Image Registration

For the deformable image registration, we used the Demons framework with image-guided filtering procedure presented in [13].

In general, the deformable image registration cost function E is defined in the following way:

$$E(\vec{u}) = Sim(I_R, I_M, \vec{u}) + \alpha Reg(\vec{u}) \qquad (3)$$

where I_R is the reference image, I_M is the moving image, $\vec{u}$ is the displacement field, $\alpha > 0$ is a weighting parameter, and Sim and Reg denote the similarity and regularization terms, respectively. For the Demons approach, the minimization of the cost function Eq. (3) is an iterative process that alternates between calculating *matching forces* based on the similarity term Sim, and performing the subsequent regularization Reg via a Gaussian smoothing of the estimated displacement field.

To register the corresponding volumes from the DCE-MRI sequences, we used the local correlation coefficient (LCC) as a similarity measure following its successful application to MRI data [11] and to DCE-MRI [13]. Details of the implementation for the LCC-Demons can be found in [11], and for the Demons with image-guided filtering in [13], where for the regularisation a spatially adaptive filtering of the estimated displacement field [7] was used.

The estimated displacement field $\vec{u}$ is filtered using the context of the guidance information provided by an additional auxiliary image I_G (guidance image) as follows:

$$\vec{u}_{i+1}(\vec{x}) = \sum_{\vec{y} \in \mathcal{N}_k} W_{\vec{x}\vec{y}}(I_G)\vec{u}_i(\vec{y}) \qquad (4)$$

where: $\vec{x}$ is a spatial position, $W_{\vec{x}\vec{y}}$ are image-guided filter kernel weights derived from I_G within a local patch $\mathcal{N}_k$, and i is an iteration index (see details in [7]).

For a given guidance image I_G, the kernel weights $W_{\vec{x}\vec{y}}$ at the position $\vec{x}$ are explicitly expressed as:

$$W_{\vec{xy}}(I_G) = \frac{1}{|\mathcal{N}|^2} \sum_{k:\vec{x},\vec{y}\in\mathcal{N}_k} (1+\Psi)$$
$$\Psi = \frac{(I_G(\vec{x})-\mu_k)(I_G(\vec{y})-\mu_k)}{\sigma_k^2+\epsilon} \quad (5)$$

Here, $|\mathcal{N}|$ represents the number of voxels in $\mathcal{N}_k$, μ_k and σ_k^2 are the mean and the variance of I_G in $\mathcal{N}_k$, and ϵ is the guided filter regularisation.

In [13], the guidance image was built based on a sparse image representation using supervoxel image clustering. However, the concept of filtering the estimated displacement field using image-guided filtering is more generic than the sliding motion modelling presented in [13]. The procedure of image-guided filtering applied to the estimated displacement field can efficiently make use of the biological information provided in the guidance image to perform locally adaptive regularisation. In the present study, the guidance image is built based on biological information extracted from the DCE-MRI derived descriptors presented in the previous section.

We therefore explore the use of the DCE-MRI based tumor descriptors derived following the steps given in Section 2.1 as guidance images I_G to perform an efficient spatial filtering of the deformation field using Eq.5. Such a deformation field would be expected, for instance, to demonstrate tumor expansion in proliferating areas and volume conservation or even reduction in other areas of the tumor, such as necrotic areas.

In [4], the authors defined a novel multichannel similarity measure, which minimizes the differences between volumes using DCE-MRI derived parameters extracted with the Toft's model. Here, we use DCE-MRI derived descriptors to impose prior knowledge to the regularization term, while for the similarity measure we use a common local correlation coefficient. Therefore, the novelty of our approach resides in using biologically relevant descriptors of local properties (including local estimates of cell number and oxygen level) to regularize the deformation field. We will show how this method yields improved registration as well as estimation of tumor volume growth at a future point.

3. Experiments and Results

Three mice (hereafter called Cases 1-3), in which MC38 (colon carcinoma) tumor cells were injected, were imaged at three time points ($\tau1$, $\tau2$ and $\tau3$) over the tumor growth cycle (days 21, 23 and 24 post injection). DCE-MRI imaging was performed on a 4.7T Agilent VNMRS using a respiratory-gated 3D gradient echo sequence (TE=0.6ms, TR=1.1ms, FA=5°, FOV=54x27x27mm, matrix:128x64x64) with 50-100 frames taken every 8-12s. B1 corrections for accurate flip angle estimation were performed using a respiratory-gated, steady-state maintained implementation of the actual flip angle imaging method [20], and T1 was estimated using a respiratory gated, steady-state maintained variable flip angle scan using the same imaging parameters as for the DCE-MRI scan itself. Gadolinium (Omniscan, 30 ul in 5s) was used as CA and delivered via a tail vein canula. To avoid breathing artefacts, animals were anaesthetised for bulk subject immobilisation using isoflurane (1-3%) in air, maintaining a respiration rate of 40-60 breaths per minute.

Algorithm 1: LCC-Demons with Guidance Imaging Filtering [13]

Input: Images I_R and I_M Parameters: σ_{LCC}, r and ε
Output: Displacement field $u_{\vec{new}}$
$u_{\vec{i+1}} := \vec{0}$
$i = 0$
repeat
  $u_{\vec{i+1}} := u_{\vec{i}}$
  Compute the updated matching force [11] $\vec{du}$
  Update the deformation field $u_{\vec{cur}} := u_{\vec{i}} \circ \vec{du}$
  Compute $u_{\vec{new}}$ by filtering $u_{\vec{i}}$ using tumor descriptor maps as I_G in Eq. 4
  Increment i
until (convergence of $||u_{\vec{i+1}} - u_{\vec{i}}||^2$) **or** $(i = i_{max})$
return

To allow for spatial comparison of the descriptor maps at each time point, rigid registration was performed to eliminate differences in mouse positioning[1]. The residual difference between the images was assumed to be due to tumor growth. Because the tumor descriptor maps ($cell$, $cell_p$, $cell_n$, $cell_h$ and pO_2) have different value ranges when compared with the imaging intensity values, both the 3D tumor descriptor maps and the DCE-MRI images were normalised to their maximum values over the whole image prior to registration. For each of the three preclinical cases deformable registration using diffeomorphic logDemons with a local correlation coefficient (LCC) as a similarity criterion was performed [11] between τ_1 and τ_2, τ_2 and τ_3, and τ_1 and τ_3 to serve as a reference for comparison with the guided-image registration approach proposed in this study.

To calculate the local correlation coefficient a smoothing parameter $\sigma_{LCC} = 4$ was employed. For the filtering of the displacement field, a guided filter radius of $r = 2$, comprising a local patch size of 5x5x5, and a guided filter regularisation of $\varepsilon = 0.01$ were used.

[1]The Image Registration Toolkit was used under Licence from Ixico Ltd https://www.doc.ic.ac.uk/~dr/software/index.html

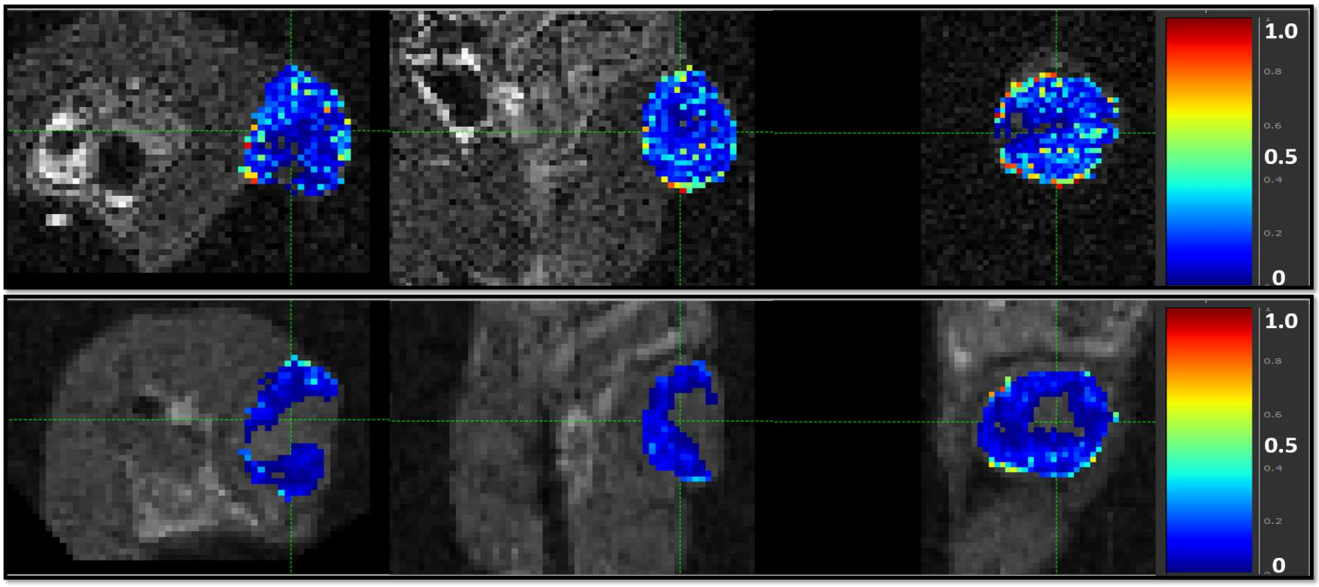

Figure 2. DCE-MRI overlaid with the descriptor maps $cell_h$ for τ_2 (top row) and τ_3 (bottom row) for Case 1, used for the registration between τ_1/τ_2; and τ_2/τ_3 and τ_1/τ_3, respectively.

Table 1. Assessment of the variability for the descriptors over the tumor volume based on the standard deviation values for all descriptors for τ_1 (columns 2-6) and τ_2 (columns 7-11) for all three cases. Values in bold highlight the highest values for $cell(\tau_2)$ and $cell_n(\tau_2)$ representing the highest variability and hence the most heterogeneous descriptors for τ_2. Values in italic highlighting the descriptor $pO_2(\tau_2)$ represents the lowest variability and hence the most homogeneous descriptor.

Case	$cell(\tau_1)$	$cell_p(\tau_1)$	$cell_n(\tau_1)$	$cell_h(\tau_1)$	$pO_2(\tau_1)$	$cell(\tau_2)$	$cell_p(\tau_2)$	$cell_n(\tau_2)$	$cell_h(\tau_2)$	$pO_2(\tau_2)$
Case 1	0.078	0.075	0.077	0.194	0.169	**0.214**	0.170	**0.195**	0.093	*0.044*
Case 2	0.117	0.100	0.122	0.197	0.190	**0.230**	0.185	**0.196**	0.135	*0.093*
Case 3	0.103	0.038	0.100	0.165	0.138	**0.194**	0.170	**0.180**	0.146	*0.102*

Table 2. DSC overlap (%) for rigid registration, LCC-Demons deformable registration [11] and Demons registration with guidance of different DCE-MRI tumor descriptors [13]. We perform the comparison between each of the time points, aligning the earlier time points (τ_1 and $\tau 2$) to their subsequent time points (τ_2 and τ_3), where τ_1/τ_2, τ_2/τ_3 and τ_1/τ_3 represent the τ_1 to τ_2, τ_2 to τ_3 and τ_1 to τ_3 registrations, respectively. The results show that for all cases, the use of guidance to regularise the deformation field improved the Demons registration accuracy. From all descriptors, $cell$ has given the best results, followed by $cell_n$ and $cell_p$.

	Case 1			Case 2			Case 3		
Registration	τ_1/τ_2	τ_2/τ_3	τ_1/τ_3	τ_1/τ_2	τ_2/τ_3	τ_1/τ_3	τ_1/τ_2	τ_2/τ_3	τ_1/τ_3
$Rigid$	74.45	70.62	58.51	66.05	71.64	54.99	71.16	81.94	66.97
$Demons$ [11]	90.67	89.77	91.05	87.26	88.01	86.06	90.62	90.91	92.26
$cell$	92.79	90.16	90.77	**87.88**	89.43	**89.62**	**91.18**	**92.01**	**92.82**
$cell_p$	92.01	**90.17**	**91.13**	87.53	88.79	86.02	90.71	91.77	92.30
$cell_n$	**92.80**	90.10	90.82	87.80	**89.51**	87.93	91.16	91.74	**92.82**
$cell_h$	92.11	89.91	90.51	87.23	89.28	86.27	90.80	91.28	92.26
pO_2	91.53	89.78	91.05	87.51	88.56	85.85	90.70	91.03	92.28

Results

To allow for the assessment of the registration performance using either of the tumor descriptor maps, we used the Dice similarity coefficient DSC, defined as $DSC = \frac{2|A \cap B|}{A+B}$, where A is the reference image (i.e. tumor region of the earlier time points τ_1 and τ_2) and B the target image (i.e. tumor region of the subsequent time points τ_2 and τ_3). To illustrate the added value of our approach, the DSC values obtained using each of the tumor descriptor maps as guidance image are compared with the DSC values obtained after rigid registration only and using the

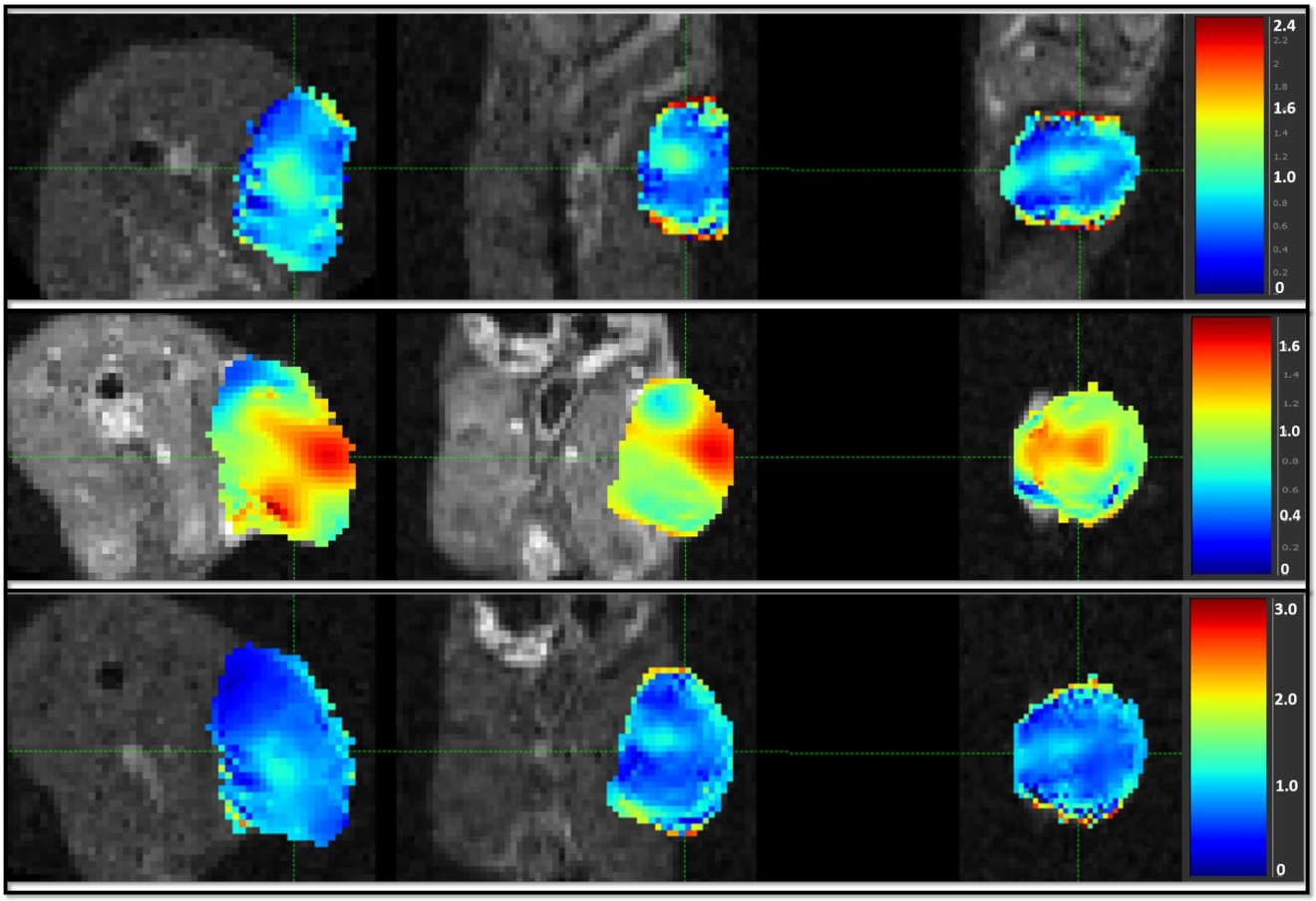

Figure 3. DCE-MRI overlaid with the determinant of the Jacobian of the estimated displacement field obtained using $cell_h$ as guidance image for the registration between τ_1/τ_2 (top row), τ_2/τ_3 (middle) and τ_1/τ_3 for Case 1. The higher Jacobian values (¿1) can be mainly observed in the tumor peripheries where the highest level of proliferation and hence growth is expected. Values close to 1 and smaller than 1 representing volume preservation and shrinkage, respectively, can be seen in the inner core of the tumor.

Table 3. Relative volume difference (%) between Jacobian based estimation and ground truth tumor delineation volumes for LCC-Demons deformable registration [11] and Demons registration with guidance of different DCE-MRI tumor descriptors [13]. We perform the comparison between each of the time points, aligning the earlier time points (τ_1 and $\tau 2$) to their subsequent time points (τ_2 and τ_3), where τ_1/τ_2, τ_2/τ_3 and τ_1/τ_3 represent the τ_1 to τ_2, τ_2 to τ_3 and τ_1 to τ_3 registrations, respectively. The results show that using the descriptors hypoxic cells ($cell_h$) and level of oxygen (pO_2) as guidance images achieved better results in terms of volume change estimation.

	Case 1			Case 2			Case 3		
Registration	τ_1/τ_2	τ_2/τ_3	τ_1/τ_3	τ_1/τ_2	τ_2/τ_3	τ_1/τ_3	τ_1/τ_2	τ_2/τ_3	τ_1/τ_3
$Demons$ [11]	-16.40	-2.20	-16.84	-15.22	**-27.97**	-32.35	-12.16	-12.42	-25.49
$cell$	-16.90	-2.23	-16.70	-14.38	-41.87	-32.88	-12.17	-15.70	-25.13
$cell_p$	-15.86	-2.61	-16.09	-15.33	-31.06	-32.41	-12.20	-13.91	-25.51
$cell_n$	-17.47	-2.84	-16.88	-14.47	-37.89	-33.68	-12.40	-15.27	-25.22
$cell_h$	**-15.45**	-2.18	**-14.15**	**-14.33**	-34.42	**-31.73**	**-11.72**	**-12.06**	**-24.84**
pO_2	-15.58	**-2.17**	-15.71	-14.83	-29.04	-33.01	-11.84	-12.21	-25.32

state-of-the-art LCC-Demons registration [11]. Results for all methods are listed in Tab. 2.

For all cases, the use of guidance images yielded better results than the LCC-Demons registration [11]. Apart from Case 1 (τ_1 to τ_3) and Case 2 (τ_1 to τ_3), the use of any of tumor descriptors as guidance images yielded higher DSC overlap than using LCC-Demons registration without a guidance image or rigid registration alone. From all tumor descriptors, the relative number of total tumor cells ($cell_p$) has resulted in the best outcome in terms of DSC overlap

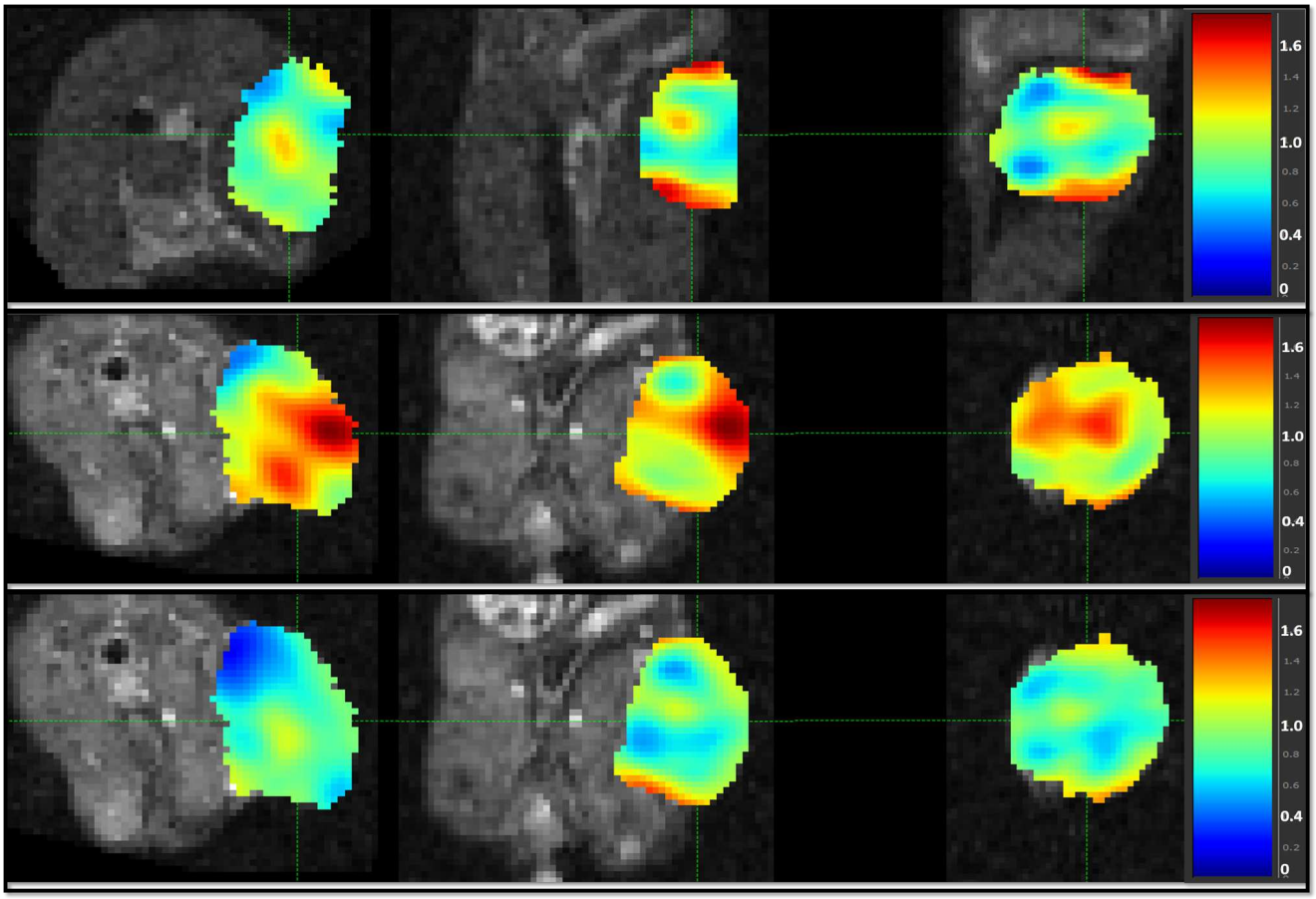

Figure 4. DCE-MRI overlaid with the determinant of the Jacobian of the estimated displacement field obtained using LCC-Demons deformable registration [11] for the registration between τ_1/τ_2 (top row), τ_2/τ_3 (middle) and τ_1/τ_3 for Case 1. When compared with Fig.3 more homogeneous Jacobian maps and lower maximum values can be observed.

(for 5 out of the 9 registrations). This is followed by the relative number of necrotic (3 out of 9) and proliferative cells (2 out of 9). For Case 3 using $cell$ as a guidance image yielded the best results for all three registrations, τ_1 to τ_2, τ_2 to τ_3 and τ_1 to τ_3.

To explore the connection between the input maps and the registration outcome in terms of DSC overlap, Fig. 1 shows the descriptor maps for one slice for each of the cases for τ_2. Additionally, Tab. 1 displays the standard deviation values for each of the descriptors across the tumor volume. For all three cases, pO_2 was the descriptor which yielded the lowest DSC (yet still better than the state-of-the-art LCC-Demons registration [11], as shown in Tab. 2). In Fig. 1, pO_2 is shown to be the most homogeneous descriptor, which also displays the lowest standard deviation value as shown in Tab. 1 (column 11). In contrast, $cell$ and $cell_n$, whose use as image guidances resulted in the highest DSC values, appear to have the most heterogeneous maps (shown in columns 1 and 3 of Fig. 1 and columns 7 and 9 in Tab. 1).

To evaluate tumor growth, the determinant of the Jacobian of the estimated displacement fields was computed. Cases 1 and 3 display better results than Case 2 in terms of estimation of the volume measured by the integration over the Jacobian. The results listed in Tab. 3, which represent the relative error between the volume change estimated via the Jacobian of the deformation field and the volume calculation from ground truth tumor delineations (manual delineation performed by a radiologist), demonstrate an underestimation of the volume for all cases (represented by the negative values). Except Case 2 (τ_2 to τ_3 and τ_2 to τ_3), using the descriptors $cell_h$ and pO_2 yielded better volume estimations than using the state-of-the-art LCC-Demons registration [11]. For 6 out of the 9 registrations performed, using $cell_h$ as a guidance image resulted in the smallest relative volume estimation error.

To investigate the connection between the use of $cell_h$ as guidance images and the determinant of the Jacobian of the estimated displacement field, the $cell_h$ maps used for the registration between τ_1/τ_2; and τ_2/τ_3 and τ_1/τ_3 for Case 1 are shown in Fig.2 in the first and second rows, respectively.

The maps for τ_1 (first row) depict a more heterogeneous structure than the maps for τ_2 (second row). A more heterogeneous map holds more local information for the regularization of the deformation field. This can be observed as a higher difference between the Jacobian maps obtained using $cell_h$ as guidance image (Fig. 3) and the ones obtained using LCC-Demons deformable registration [11] Fig. 4 for the registration between τ_1/τ_2 (top rows) and τ_1/τ_3 (bottom rows) for Case 1. The Jacobian maps in Fig. 3 indicate considerable volume expansion in the outer parts of the tumor and volume shrinkage and preservation in the interior parts including necrotic and hypoxic areas. In contrast, the Jacobian maps in Fig. 4 depict a slight, homogeneous volume expansion across the whole tumor.

4. Discussion and Conclusions

In this study we have presented a novel method for deformable registration in the presence of tumor which uses tumor descriptor maps as guidance images within a Demons framework [13]. The method includes the novel regularization model of the displacement field based on spatial physiological information derived from DCE-MRI data. Such a method yields better registration results than the state-of-the-art LCC-Demons registration [11] (shown by the higher DSC values recorded in Tab. 2) while also allowing for an image-based quantification of local and total tumor growth, which demonstrates physiologically meaningful tumor expansion (e.g. in proliferating areas) and volume conservation or reduction (e.g. necrotic areas).

The results serve as a proof of concept and have demonstrated the feasibility of using tumor descriptors derived from DCE-MRI data to aid registration in the presence of a tumor. The descriptors introduced in this study have shown the potential to estimate tumor volume evolution, which could be used in radiology as a volumetric approach to characterize tumor progression or regression instead of the simple yet inaccurate RECIST method. Moreover, DCE-MRI based descriptors, as the ones introduced here, can serve as an adjunct to determine tumor progression or regression.

The proposed method is shown to yield better results in terms of higher DSC overlap for more heterogeneous tumors (e.g. the one presented in Case 2). The proposed framework seems to be mostly suitable to retrieve tumor volume change for more heterogeneous tumors (e.g. the one presented in Case 1). The fact that descriptors demonstrating a more heterogeneous behaviour yielded improved results in terms of both registration performance and tumor volume estimation, suggests that the tumor tissue with its heterogeneous structure plays an important role in tumor growth. Perfusion (or the lack of it) represented in this study by the tumor descriptors pO_2 and $cell_h$ is not only crucial in further *in vivo* tumor growth but seems to be an indicative of tumor growth assessed via medical imaging.

Another advantage of the proposed method over other methods such as the one proposed by [4] lies in the fact that the obtained Jacobian maps (such as the one shown in Fig. 3) can be interpreted physiologically. Similarly to the maps in Fig. 4 obtained using the LCC-Demons deformable registration [11], the Jacobian maps of the deformation field obtained in [4] displayed a stretching of the necrotic core (represented by the higher Jacobian values). This stretching is partially artificial in that it does not take into account the tumor expansion happening due to proliferation in the tumor outer rim. Our method, which resulted in higher Jacobian values shown in the proliferative rim for all three cases seems to successfully account for the heterogeneity of local tumor growth and regression. Such physiologically meaningful Jacobian 3D maps could for instance aid physicians in the development of therapy strategies to deliver different doses of radiation to different areas of the tumor. The positive impact would be twofold: bolster therapy effectiveness in areas where cells are proliferating while avoiding unnecessary delivery of therapy to tumor areas which are already responding and thus shrinking. This could potentially reduce unnecessary use of radiation-intensive therapy, saving resources and reducing the strain such therapies place on patients. A current limitation of our approach is that it makes several assumptions to transform DCE-MRI parameters into tumor descriptors. Given the novelty of the methods used, in order to show that this proof of principle is sound, a comparison of the tumor descriptors to histopathological data will be included in the future.

The fact that different descriptors achieved better results for DSC overlap ($cell$ and $cell_{nec}$) and volume estimation ($cell_h$ and pO_2), combination of these descriptors could be used in a multichannel guidance approach [13] to explore whether the descriptors can have a complementary effect on the results, thus optimising both the DSC overlap and tumor volume estimation.

To overcome the challenge that changes caused by tissue death and tumor growth pose on registration, a model of tumor growth accounting for cell proliferation and death will be embedded into the registration framework in an iterative manner. Once clinically validated, such a model-based registration approach is expected to not only improve registration, serve as volumetric and functional assessment of tumor burden, but also to be a step towards the development of personalized, patient-specific tumor treatment.

5. Acknowledgements

We would like to acknowledge funding from the CRUK/EPSRC Oxford Cancer Imaging Centre. Figures were generated using PkView our in-house DCE-MRI analysis software (http://pkview.readthedocs.org/en/latest/) which was developed for tumour subregional analysis [10].

References

[1] V. Adhikarla and R. Jeraj. An imaging-based stochastic model for simulation of tumour vasculature. *Physics in medicine and biology*, 57(19):6103–24, Oct. 2012. 3

[2] N. C. Atuegwu, L. R. Arlinghaus, X. Li, a. B. Chakravarthy, V. G. Abramson, M. E. Sanders, and T. E. Yankeelov. Parameterizing the Logistic Model of Tumor Growth by DW-MRI and DCE-MRI Data to Predict Treatment Response and Changes in Breast Cancer Cellularity during Neoadjuvant Chemotherapy. *Translational Oncology*, 6(3):256–264, June 2013. 2

[3] M. Bhushan, J. A. Schnabel, L. Risser, M. P. Heinrich, M. Brady, and M. Jenkinson. Motion correction and parameter estimation in dcemri sequences: application to colorectal cancer. *Medical Image Computing and Computer-Assisted Intervention, MICCAI*, pages 476–483, 2011. 2

[4] M. Enescu, A. Cifor, V. Kersemans, D. Allen, S. Gilchrist, J. Beech, S. Smart, M. A. Chappell, and J. A. Schnabel. Pharmacokinetic Modelling of Longitudinal DCE-MRI Scans for Assessment of Tumour Growth. In *Intl. Soc. Mag. Reson. MEd*, volume 22, page 1126, 2014. 4, 8

[5] O. Fernández-Guinea, A. Andicoechea, L. O. González, S. González-Reyes, A. M. Merino, L. C. Hernández, A. López-Muñiz, P. García-Pravia, and F. J. Vizoso. Relationship between morphological features and kinetic patterns of enhancement of the dynamic breast magnetic resonance imaging and clinico-pathological and biological factors in invasive breast cancer. *BMC cancer*, 10:8, 2010. 2

[6] V. Hamy, N. Dikaios, S. Punwani, A. Melbourne, J. Latifoltojar, A. adn Makanyanga, C. M., H. E., A. Manys, T. S., and A. D. Respiratory motion correction in dynamic mri using robust data decomposition registrationapplication to dce-mri. *Medical Image Analysis*, 18:301–313, 2014. 2

[7] K. He, J. Sun, and X. Tang. Guided image filtering. *Pattern Analysis and Machine Intelligence, IEEE Transactions*, 2013. 3

[8] M. Heilmann, C. Walczak, J. Vautier, J. L. Dimicoli, C. D. Thomas, M. Lupu, J. Mispelter, and A. Volk. Simultaneous dynamic T1 and T2* measurement for AIF assessment combined with DCE MRI in a mouse tumor model. *Magma (New York, N.Y.)*, 20:193–203, 2007. 2

[9] E. Hodneland, E. A. Hanson, A. Lundervold, J. Modersitzki, E. Eikefjord, and A. Z. Munthe-Kaas. Segmentation-driven image registration-application to 4d dce-mri recordings of the moving kidneys. *Image Processing, IEEE Transactions*, 23:2392–2404, 2014. 2

[10] B. Irving, J. M. Franklin, B. W. Papiez, E. M. Anderson, R. A. Sharma, F. V. Gleeson, S. M. Brady, and J. A. Schnabel. Pieces-of-parts for supervoxel segmentation with global context: Application to DCE-MRI tumour delineation. *Medical Image Analysis*, 32:69–83, 2016. 8

[11] M. Lorenzi, N. Ayache, G. Frisoni, and X. Pennec. Lcc-demons: a robust and accurate symmetric diffeomorphic registration algorithm. *Neuroimage*, 81:480, 2013. 3, 4, 5, 6, 7, 8

[12] M. R. Orton, J. a. D'Arcy, S. Walker-Samuel, D. J. Hawkes, D. Atkinson, D. J. Collins, and M. O. Leach. Computationally efficient vascular input function models for quantitative kinetic modelling using DCE-MRI. *Physics in medicine and biology*, 53(5):1225–1239, 2008. 2

[13] B. W. Papiez, J. Franklin, M. P. Heinrich, F. V. Gleeson, and J. A. Schnabel. Liver motion estimation via locally adaptive over-segmentation regularization. *Medical Image Computing and Computer-Assisted Intervention, MICCAI*, pages 427–434, 2015. 3, 4, 5, 6, 8

[14] A. Sotiras, C. Davatzikos, and N. Paragios. Deformable medical image registration: A survey. *Medical Imaging, IEEE Transactions*, 32:1153–1190, 2013. 1

[15] S. P. Sourbron and D. L. Buckley. Classic models for dynamic contrast-enhanced MRI. *NMR in Biomedicine*, 26(February):1004–1027, 2013. 2

[16] P. S. Tofts, G. Brix, D. L. Buckley, J. L. Evelhoch, E. Henderson, M. V. Knopp, H. B. W. Larsson, T.-y. Lee, N. A. Mayr, G. J. M. Parker, R. E. Port, J. Taylor, and R. M. Weisskoff. Contrast-Enhanced T 1 -Weighted MRI of a Diffusable Tracer : Standardized Quantities and Symbols. *Journal of magnetic resonance imaging : JMRI*, 232(10):223–232, 1999. 2

[17] P. S. Tofts and a. G. Kermode. Measurement of the blood-brain barrier permeability and leakage space using dynamic MR imaging. 1. Fundamental concepts. *Magnetic resonance in medicine*, 17(2):357–67, Feb. 1991. 2

[18] P. Van Meerten, H. Gelderblom, and J. Bloem. Recist revised: Implications for the radiologist. a review article on the modified recist guideline. *European Radiology*, 20:1456–1467, 2010. 1

[19] O. Wu, L. Ostergaard, R. M. Weisskoff, T. Benner, B. R. Rosen, and A. G. Sorensen. Tracer arrival timing-insensitive technique for estimating flow in MR perfusion-weighted imaging using singular value decomposition with a block-circulant deconvolution matrix. *Magnetic resonance in medicine*, 50(1):164–74, 2003. 2

[20] V. L. Yarnykh. Actual flip-angle imaging in the pulsed steady state: a method for rapid three-dimensional mapping of the transmitted radiofrequency field. *Magnetic resonance in medicine*, 57(1):192–200, Jan. 2007. 4

[21] E. I. Zacharaki, C. S. Hogea, D. Shen, G. Biros, and C. Davatzikos. Non-diffeomorphic registration of brain tumor images by simulating tissue loss and tumor growth. *Neuroimage*, pages 762–774, 2009. 1

[22] B. K. L. Zierler. Circulation Research. XVI(4):309–322, 1965. 2